Changes in External Forcings Drive Divergent AMOC Responses Across CESM Generations

Michael R. Needham[1], **Douglas D. Falter**[2], **David A. Randall**[1]

[1]Department of Atmospheric Science, Colorado State University
[2]Department of Geologicla and Atmospheric Sciences, Iowa State University

Key Points:

- The AMOC response to historic aerosol forcing in CESM2 depends strongly on whether CMIP5 or CMIP6 inputs are applied
- The 1940-1985 trend in the AMOC is indistinguishable between CESM1 and CESM2 when both models are run with CMIP5 forcings
- Divergent AMOC responses in CESM2-LE vs CESM2-CMIP5 are explained by differences in turbulent heat fluxes over the subpolar north Atlantic

Corresponding author: Michael Needham, `m.needham@colostate.edu`

Abstract

The Atlantic meridional overturning circulation (AMOC) in many CMIP6 models has been shown to be overly-sensitive to anthropogenic aerosol forcing, and it has been speculated that this is due to the inclusion of aerosol indirect effects for the first time in many models of that generation. We analyze the AMOC response in a newly-released ensemble of historic simulations performed with CESM2 and forced by the older CMIP5 input datasets (CESM2-CMIP5). This AMOC response is then compared to the CESM1 large ensemble (CESM1-LE, forced by the older CMIP5 inputs) and the CESM2 large ensemble (CESM2-LE, forced by the newer CMIP6 inputs). A key conclusion, only made possible by this experimental setup, is that changes in modeled aerosol-indirect effects cannot explain the differences in turbulent fluxes between CESM1-LE and CESM2-LE. Instead, differences in surface turbulent heat fluxes from changes in model inputs likely drive the different AMOC responses.

Plain Language Summary

The Atlantic meridional overturning circulation (AMOC) is important for the wider climate because it transports a large amount of warm water northward away from the equator. The most recent generation of climate models disagree with the observed behavior of the AMOC over the twentieth century, and it has been suggested that this is due to the inclusion of additional cloud processes in many of the newest models. Here we look at model simulations of the AMOC in several configurations to show that the disagreement in the past AMOC behavior is instead primarily due to changes in the inputs given to the models, rather than to changes in the models themselves.

1 Introduction

The Atlantic meridional overturning circulation (AMOC; Rahmstorf, 2002) is crucial in determining the local climate of the regions bordering the north Atlantic. It also plays a key role in the wider climate by accomplishing a significant portion of the necessary poleward energy transport determined by the TOA radiation balance (Trenberth & Caron, 2001; Chiang et al., 2008; Frierson et al., 2013; Marshall et al., 2013; Trenberth & Fasullo, 2017). The future behavior of the AMOC is of great interest because of its important role in the climate system: it has been identified as a potential climate “tipping point,” (Broecker, 1987; Lenton et al., 2019; Brovkin et al., 2021; Ditlevsen & Ditlevsen, 2023), with the potential for a slowdown or collapse of the AMOC due to greenhouse gas-induced changes in the heat and salinity budgets of the north Atlantic.

Indirect observational and proxy-based estimates suggest that the AMOC has entered a period of decline, with a general slowdown relative to the pre-industrial era, particularly over the course of the twentieth century (Rahmstorf et al., 2015; Thornalley et al., 2018; Caesar et al., 2018, 2021). In contrast, many models that participated in the most recent phase of the coupled model inter-comparison project (CMIP6; Eyring et al., 2016) predicted an *increase* in the strength of the AMOC over much of the twentieth century, likely due to the models’ overly-sensitive response to anthropogenic aerosol forcing (Menary et al., 2020; Hassan et al., 2021; Robson et al., 2022). These CMIP6 models also disagree with the older models of the CMIP5 generation, which more closely match observational AMOC estimates (Cheng et al., 2013; Menary et al., 2020).

The importance of the AMOC to the climate, and this significant model-observation disagreement motivate us to understand why models that participated in CMIP6 tend to overestimate the AMOC response to historic aerosol forcing. One hypothesis is that the first-time inclusion of aerosol-cloud interactions in many CMIP6 models (Wang et al., 2021) led to cooling of the northern relative to the southern hemisphere, which induced an increase in the strength of the AMOC (Menary et al., 2020). In this study we analyze a different hypothesis that has not yet been investigated to our knowledge: our goal is to quantify to what extent the change in external forcings from CMIP5 to CMIP6 contributes to the divergent AMOC responses of the CMIP5 and CMIP6 models. This hypothesis does not contradict the aerosol-cloud interaction hypothesis: both can contribute.

2 Data

We utilize three ensembles of coupled historical (1850- or 1920-present) simulations performed with the first (CESM1; Hurrell et al., 2013) or the second (CESM2; Danabasoglu et al., 2020) version of the Community Earth System Model at a nominal 1° horizontal atmospheric resolution. The first is a set of 35 simulations from the CESM1 large ensemble project using CMIP5 forcings (hereafter CESM1-LE; Kay et al., 2015); the second is 50 of the 100 simulations from the CESM2 large ensemble project using CMIP6 forcings (hereafter CESM2-LE; Rodgers et al., 2021); the third is 10 of the 15 simulations (only 10 simulations included all necessary fields at the time of analysis) performed using CESM2 but forced by the older CMIP5 inputs (hereafter CESM2-CMIP5; Holland et al. (2023)). We use only the 50 members of the CESM2-LE which utilize smoothed biomass burning rather than the native CMIP6 biomass burning, because the later has been shown to lead to anomalous northern hemisphere warming towards the end of the historical period (Fasullo et al., 2022). We note that the smoothed biomass burning forcing only deviated from the standard CMIP6 forcing after 1990 (due to the 11 year smoothing filter, see Rodgers et al., 2021), which occurs after the primary peak in the AMOC anomaly in CMIP6 models.

These three experimental configurations allow us to separate the difference in AMOC response to historic forcing between CESM1-LE and CESM2-LE into two components: the difference between CESM1-LE and CESM2-CMIP5 gives the impact of changing model versions with the external inputs held constant, while the difference between CESM2-CMIP5 an CESM2-LE gives the impact of changing the forcing from CMIP5 to CMIP6 in the same version of the model. Crucially, the CESM1 large ensemble employed the community atmosphere model version 5, which *does* include a representation of aerosol-cloud interactions (Hurrell et al., 2013; Kay et al., 2015), although the treatment of these interactions is different between CESM1 and CESM2 (Danabasoglu et al., 2020). Specifically, the atmospheric component of CESM2 utilizes an updated cloud microphysics scheme (MG2; Gettelman & Morrison, 2015) and an updated, four-mode aerosol model (MAM4; Liu et al., 2016).

All fields are ensemble means calculated from monthly mean model output. Annual mean timeseries anomalies are first computed by calculating monthly anomalies from the 20-year climatology defined as 1921-1940 - the earliest period that is common to all simulations - and then calculating the average anomaly for each year. Yearly time series are then smoothed with an 11 year gaussian filter with a standard deviation of 5 years.

3 AMOC evolution and Solar Absorption

The top panel of Fig. 1 shows the time series of the ensemble mean AMOC index anomaly for each of the three sets of simulations. The AMOC index is calculated as the maximum value of the overturning streamfunction in the Atlantic basin below a depth of 500 meters. Shading shows the interquartile range among ensemble members. We use only the Eulerian component of the MOC, which is explicitly resolved by the model, although results are similar when the total (i.e., resolved plus parameterized) AMOC is analyzed (not shown).

The AMOC anomaly from the CESM2-LE (red curve) peaks in the later quarter of the twentieth century, which is consistent with other CMIP6 generation models un-

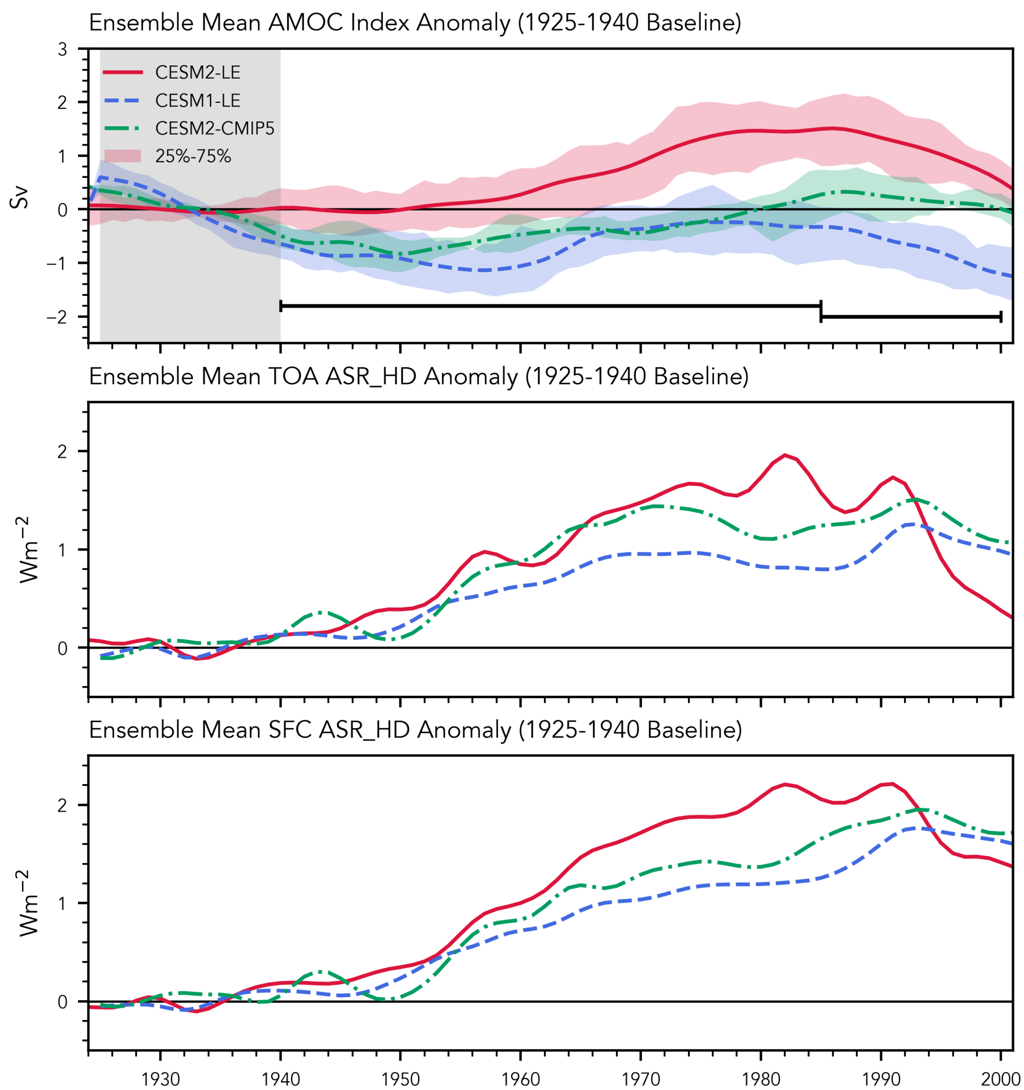

Figure 1. **Top)** Time series of the ensemble mean AMOC anomaly for three ensembles of climate simulations performed using the CESM (see text for details of model configurations and forcings) Black lines span the ranges used for calculating AMOC trends in Fig. 2. **Middle)** Ensemble mean anomaly in the hemispheric difference in absorbed solar radiation at the top of the atmosphere (ASR_HD, defined as SH minus NH). **Bottom)** as in **Middle**, but for the ASR_HD calcualted from surface shortwave fluxes.

der the standard historical forcings (Menary et al., 2020; Robson et al., 2022). The AMOC anomaly from the CESM1-LE (blue curve) is typically negative over the historical period relative to 1921-1940, which in turn is consistent with other CMIP5 models. This establishes that CESM1 under CMIP5 and CESM2 under CMIP6 forcings are at least nominally representative of the wider CMIP5 and CMIP6 population of models discussed by Menary et al. (2020).

The AMOC anomaly from the CESM2-CMIP5 simulations (green curve) much more closely follows the CESM1-LE curve rather than the CESM2-LE curve from the beginning of the simulations in 1920 through to the 1980s. After about 1985 the CESM2-CMIP5 AMOC anomaly is essentially flat while both the CESM1-LE and CESM2-LE anomalies decrease at essentially the same rate. This result is the key finding of this study; it shows that the AMOC response in CESM2 is strongly dependent on the particular historical inputs (i.e., CMIP5 vs. CMIP6 forcings) to that model. It also establishes that the difference in AMOC response in CESN2-LE vs CESM1-LE cannot be explained by changes to the model.

Previous studies have attributed the divergent AMOC responses of the CMIP5 and CMIP6 models to enhanced northern hemispheric cooling in CMIP6 models associated with the inclusion of aerosol indirect effects. However, as mentioned in the previous section, all three ensembles analyzed here employ atmospheric models (either CAM5 or CAM6) which include representations of aerosol-cloud interactions, yet we still observe a large difference in the AMOC response between the two ensembles forced with CMIP5 inputs and the CESM2-LE, which is forced by CMIP6 inputs.

The middle and bottom panels of Fig. 1 show the difference (SH minus NH) in the hemispherically averaged absorption of solar radiation at the TOA or the Surface, respectively. This metric has been shown to exhibit a high degree of correlation with the AMOC index for CMIP6 models (Menary et al., 2020). Physically, a more reflective northern hemisphere would indicate a hemispheric difference in solar heating, which would require anomalous cross-equatorial heat transport by the AMOC to maintain energy balance. This metric is not an exact proxy for the AMOC because atmospheric processes are also able to transport anomalous energy across the equator to balance the hemispheric difference in solar heating (Chiang & Bitz, 2005; Donohoe et al., 2013; Bischoff & Schneider, 2014; Lembo et al., 2019; Irving et al., 2019; Yukimoto et al., 2022; Pearce & Bodas-Salcedo, 2023; Needham & Randall, 2023). Nonetheless the metric is a useful measure of the energetic influences on the AMOC and the wider climate over the twentieth century. Interestingly the three model configurations more-or-less agree on the temporal evolution of ASR_HD anomaly, contrary to their disagreement on the sign of the AMOC anomaly.

Together, the *disagreement* in the evolution of the AMOC anomaly and the *agreement* in the evolution of the ASR_HD anomaly indicate that the divergent AMOC response between the three CESM1-LE and CESM2-LE cannot be explained by hemispheric-wide differences in solar heating in response to aerosol forcing. This suggests a focus on more localized processes is necessary to account for the much stronger AMOC response in the CESM2-LE compared to the other two ensembles.

Figure 2 shows a comparison of the AMOC trends between the three ensembles from 1940-1985 and from 1985-2000. In the interest of a better comparison with the CESM2-CMIP5 ensemble, which includes only 10 simulations, we have taken a bootstrapping approach in which 10 simulations are chosen at random from both the CESM1-LE and CESM2-LE and the average trend from these 10 members is calculated. This process was repeated 500 times to generate the distributions of AMOC trends shown in the figure for CESM1-LE (blue) and CESM2-LE (red). The vertical green bar shows the ensemble mean trend from the 10 CESM2-CMIP5 simulations. From 1940-1985 the AMOC trend for the CESM2-CMIP5 is indistinguishable from the CESM1-LE (which uses the same CMIP5 forcings),

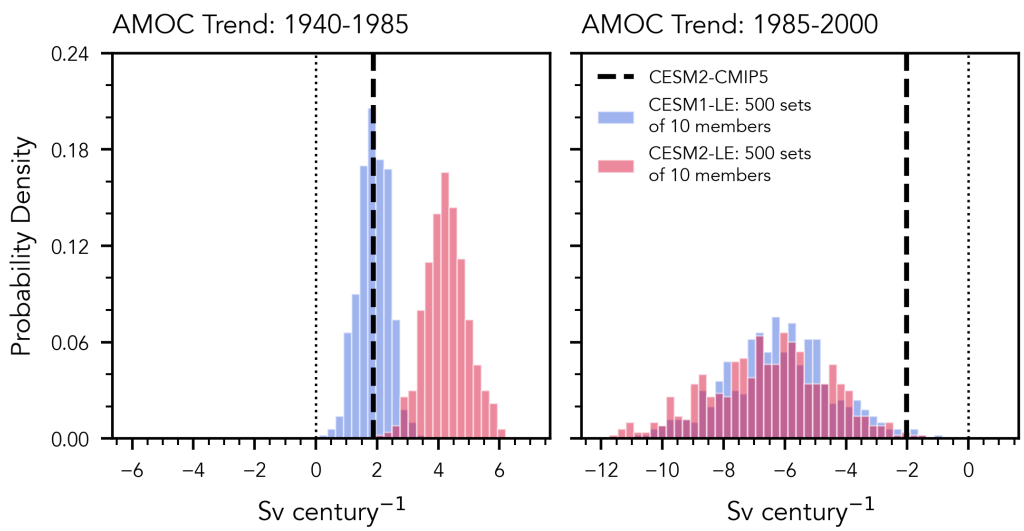

Figure 2. **Left)** comparison of AMOC trends from 1940-1985 for each of the CESM large ensembles. **Right)** as in **Left)** but for the trend from 1985-2000. PDFs were calculated from a bootstrapping approach where the mean AMOC trend from 10 random ensemble members from CESM1-LE or CESM2-LE2 were interactively calculated to align with the 10 ensemble members from the CESM2-CMIP5. Vertical black dashed line in each panel represents the average CESM2-CMIP5 trend for the period.

and is clearly different from the CESM2-LE (which uses the different CMIP6 forcings). From 1985-2000 the trends in the two large ensembles are indistinguishable, with similar model spread, while the CESM2-CMIP5 trend decreases at a much slower rate of about 2 Sv per century.

The bottom-left panel of Fig. 3 shows the climatological (black contours) and anomalous (shaded contours) overturning streamfunction (Ψ) in the Atlantic basin for the CESM2-LE. The streamfunction has been smoothed along the latitude dimensions with a gaussian filter to facilitate the calculation of the meridional derivative. The shaded contours indicate that the anomaly in the AMOC index seen in the top panel of Fig. 1 coincides with an increase in the magnitude of the streamfunction throughout the depth of the basin. This corresponds to enhanced sinking motion in the north Atlantic, as illustrated by the bottom right panel of Fig. 1, which shows the anomalous vertical mass flux (M_z) associated with the change in the streamfunction, calculated as

$$M_z = \frac{1}{a\cos\varphi}\frac{\partial\Psi}{\partial\varphi}. \tag{1}$$

There are two primary regions of anomalous sinking motion associated with the large AMOC anomaly in the CESM2-LE. The first occurs from 40-50°N and is likely associated with deep water formation in the Labrador sea, while the second occurs further north (near 60°N), and is likely associated with deep water formation in the Greenland sea. Sinking water in both of these regions are canonically understood to contribute to the AMOC Rahmstorf (2002).

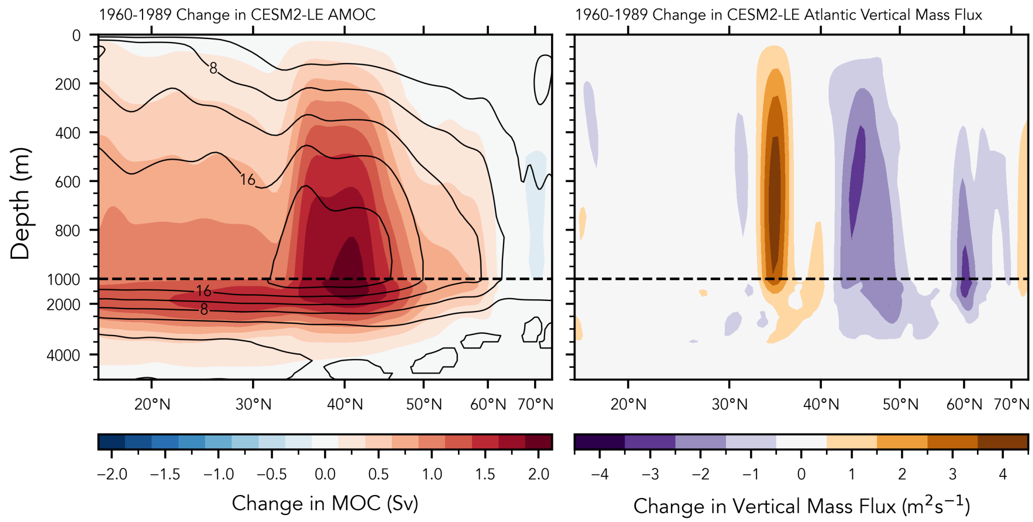

Figure 3. **Left)** CESM2-LE ensemble mean climatology (contours, 1921-1940) and anomaly (shading, 1960-1989) the overturning streamfunction in the Atlantic basin. **Right)** Anomaly in the vertical mass flux implied by the anomaly in the streamfunction as seen in the **Left** panel. Note the irregular y axes of the panels in the bottom row, used to emphasize the behavior in the top 1000 meters (with the shift between scales marked by the horizontal dashed line).

4 Energy Budget of the North Atlantic

The AMOC is primarily driven by a meridional pressure gradient that is maintained by the sinking of relatively cold and salty surface water in the north Atlantic (Rahmstorf, 2002), as seen in Fig. 3. This rate of sinking is determined by the sea-surface density, so it is sensitive to processes which alter the density. In principle, the sea-surface density can be altered by thermal (i.e., temperature-changing) or haline (i.e., salinity-changing) processes (e.g., Speer & Tziperman, 1992): in practice, we find that thermal processes are much more important for altering the sea-surface density (not shown), consistent with Robson et al. (2022). Therefore, to better understand which processes drive the enhanced sinking motion seen in Fig. 3, we now investigate the energy budget of the north Atlantic.

The top row of Fig. 4 shows the average anomaly (1960-1989, relative to the 1921-1940 climatology) of the net heat flux over the north Atlantic. It is immediately obvious that CESM2-LE has a much larger heat flux anomaly than either the CESM1-LE or the CESM2-CMIP5. The spatial pattern is also different, with CESM2-LE producing negative anomalies across the entire north Atlantic, while CESM1-LE and CESM2-CMIP5 have a similar spatial structure with varying positive and negative anomalies. The middle row of the same figure shows the ensemble mean sensible plus latent turbulent heat flux. It is clear that the spatial structure of the surface heat flux anomaly (i.e., the top row) is primarily determined by turbulent surface fluxes, and not by surface radiation fluxes (i.e., the bottom row). In the following figure we further decompose the energy budget into its constituent parts and look at its time evolution.

Panels a-g of Fig. 5 show the time series for each of the components of the surface energy budget (and various combinations thereof) averaged over the subpolar north Atlantic (the boundary of the region is specified in the cpation of Fig. 4). We will refrain

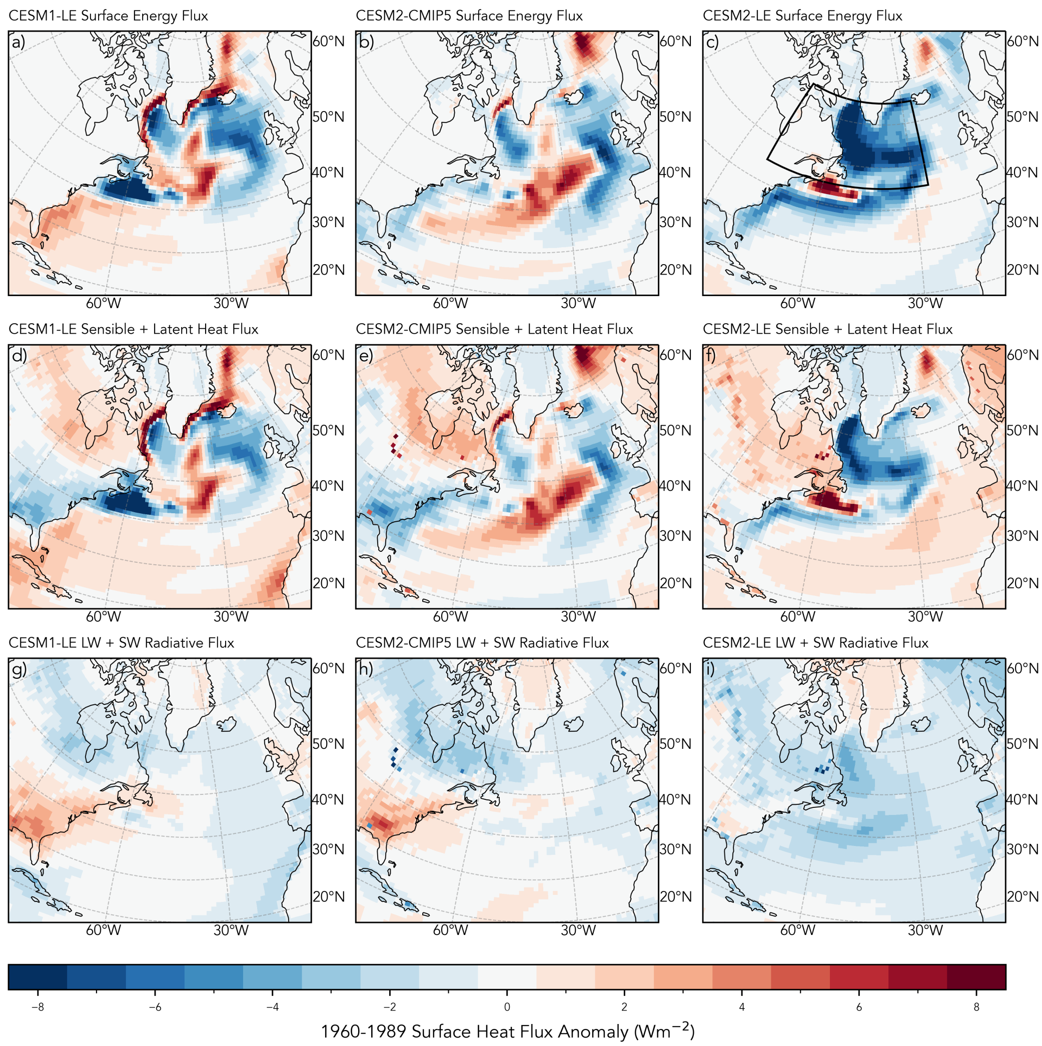

Figure 4. **Top Row)** Ensemble mean anomaly (1960-1989) in the net energy balance in the north Atlantic for the CESM1-LE, CESM2-CMIP5, and CESM2-LE ensembles, (left, center, and right columns, respectively). **Middle Row)** as in **Top Row** but for the anomaly in the net sensible plus latent turbulent heat flux. **Bottom Row)** as in **Top Row** but for the anomaly in the net longwave plus shortwave radiative flux at the surface. Negative (blue) values indicate an anomalous *heat loss* out of the ocean. The black boxed region in **panel c** indicates the region used for spatial averages in Fig. 4, and is bounded by 80°W-25°W and 45°N-65°N.

from discussiong each panel individually because only certain terms turn out to be important. Instead we present several key findings from this figure.

The first is that the CESM1-LE (blue dashed curves) and the CESM2-CMIP5 (green dash-dotted curve) largely agree on the behavior of each of the terms in the energy budget, and both of these ensembles *disagree* with the CESM2-LE when the term of interest is large (e.g., panels a and g). This underscores the key conclusion of this study that the difference in the AMOC response between the CESM1-LE and CESM2-LE is largely due to a change in forcing rather than to a change in the model. The second conclusion is that the disagreement in the net surface energy flux (panel g) is largely explained by the disagreement in the turbulent heat fluxes (panel a) with only a small contribution from differences in radiative fluxes (panel d). Our third conclusion from the surface energy budget is that the disagreement in the turbulent fluxes (panel a) is largely due to differences in the latent heat flux (panel b) although the contribution from sensible heat fluxes is non-negligible.

Beyond the decomposition of the energy budget, panels h and i of Fig. 5 allow us to make two additional comments. First, we note that the shortwave cloud radiative effect (panel h) is small in this region, with little difference between the two ensembles. This does not necessarily mean that the differences in aerosol-cloud interactions are unimportant between these ensembles, but instead that differences in these interactions are *not locally important in the subpolar north Atlantic*. Second, the anomaly in the 10 meter wind speed (panel i) is extremely small, only about 0.1 $\mathrm{ms}-2$. Therefore, the changes in the turbulent surface fluxes (panels a-c) cannot be explained by dynamic changes, but must instead be thermodynamically driven. In other words, the large anomaly in the CESM2-LE turbulent heat flux is primarily driven by the thermodynamic (e.g., the air-sea difference in temperature) component rather then by a change in the winds, consistent with the conclusions of Robson et al. (2022).

5 Conclusion and Discussion

We have shown that the AMOC response in three configurations of the community earth system model is highly sensitive to external forcings. When run with CMIP6 forcings, CESM2 exhibits an increase in the strength of the AMOC from 1940-1985, consistent with many other CMIP6 models (Menary et al., 2020) and *inconsistent* with observations (Rahmstorf et al., 2015; Thornalley et al., 2018; Caesar et al., 2018, 2021). The fact that this AMOC anomaly is absent in both the CESM1-LE and when CESM2 is forced by the older CMIP5 inputs establishes that this difference cannot be explained by differences in the model but must be due in large part to a change in forcings from CMIP5 to CMIP6.

The energy budget analysis (Figs. 4-5) indicates that the stronger AMOC response in CESM2-LE is largely explained by enhanced surface fluxes of latent along with sensible heat, which led to anomalous ocean cooling from the Labrador sea, as in Hassan et al. (2021) and Robson et al. (2022). The change in the magnitude of the surface winds is small (Fig. 5), suggesting that this change in turbulent heat fluxes is thermodynamically rather than dynamically driven, consistent with Robson et al. (2022). We note that the shortwave flux anomaly is not negligible in any the ensembles, but the difference in the shortwave flux is much smaller than the difference in the turbulent heat fluxes.

The fact that this large heat flux seen in CESM2-LE (i.e., panel g of Fig. 5) anomaly is absent in CESM1-LE indicates that the turbulent heat flux anomaly is a strong contributor to the different AMOC response between CESM1-LE and CESM2-LE, as in Hassan et al. (2021) and Robson et al. (2022); the fact that it is also absent in CESM2-CMIP5 indicates that the appearance of the heat flux anomaly is primarily due to a change in external forcings. Thus we conclude that the change in forcings between CMIP5 and CMIP6

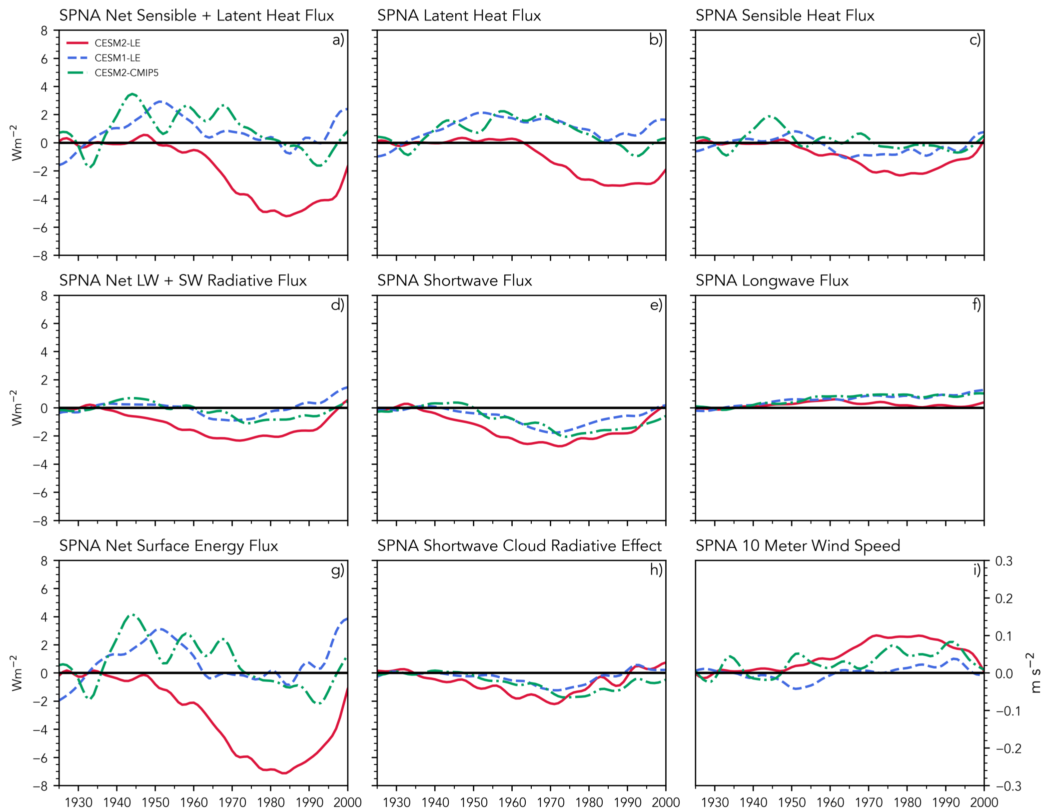

Figure 5. **Panel a)** Time series anomaly of the net sensible plus latent turbulent heat flux averaged over the subpolar north atlantic (the region bounded by the black box in **panel c** of Fig. 3, utilizing only oceanic grid cells for averages). Panels **b-g** show time series of the anomaly of additional terms of the energy budget, while panels **h** and **i** show the anomaly of the shortwave cloud radiative effect, and the 10 meter wind speed, respectively.

played a key role in the divergent AMOC response between CESM1-LE and CESM2-LE.

It is beyond the scope of this study to definitively answer why the AMOC response in CESM2 is more sensitive to CMIP6 than CMIP5 forcings, however we briefly discuss one possibility here. The CMIP5 anthropogenic emissions compiled by Lamarque et al. (2010) provided emission estimates at 10-year intervals: in contrast, the CMIP6 anthropogenic emission estimates compiled by Hoesly et al. (2018) are provided on an annual basis (see, e.g., Fig. 1 of Holland et al. (2023) or Fig. 2 of Hoesly et al. (2018)). It is conceivable, then, that the higher temporal frequency of the CMIP6 forcings led to the stronger response purely because of model sensitivity to forcing variability. Indeed, this interpretation would be consistent with Fasullo et al. (2022). They showed that a discontinuity in the variability of biomass burning forcing - which arose from the inclusion of satellite observations of wildfire emissions from 1997-2014 but not before or after that period - led to “spurious warming” near the end of historical simulations performed with CESM2. A similar sensitivity to forcing variability may explain the divergent AMOC responses presented in this study.

A key limitation of this work is that we have analyzed only a single model. This particular experimental setup (in which each ensemble utilized an atmospheric model which includes aerosol indirect effects, although with different representations) makes it impossible to comment on the role of aerosol-cloud interactions on the AMOC across CMIP6 models except to say that those interactions did not play a role in the divergent AMOC response across CESM generations. However, we have no reason to believe that similar results would not be found if other models of the CMIP6 generation were forced by CMIP5 inputs. The stark differences between the AMOC response (Fig. 1) and the heat flux anomaly over the north Atlantic (Fig. 4 and panel g of Fig. 5) in CESM2-CMIP5 and CESM2-LE would indicate that similar experiments comparing the response of CMIP6-generation models under CMIP5 inputs should be performed to better understand the impact of changing forcings. Such experiments could also help to better understand the role of the representation of aerosol-cloud interactions for those models that included those processes for the first time in CMIP6.

6 Data Availability Statement

All of the model output used in this work is freely available online:

- CESM1-LE data is available at `https://www.cesm.ucar.edu/community-projects/lens`
- CESM2-LE data is available at `https://www.cesm.ucar.edu/community-projects/lens2`
- CESM2-CMIP5 data is available at `https://www.cesm.ucar.edu/community-projects/cesm2-cmip5`

Acknowledgments

This work was supported by the National Oceanic and Atmospheric Administration through grant number NA19OAR4590155, and by the National Science Foundation through grant number AGS-1826643, both to the Colorado State University.

References

Bischoff, T., & Schneider, T. (2014, July). Energetic constraints on the position of the intertropical convergence zone. *J. Clim.*, *27*(13), 4937-4951. doi: 10.1175/JCLI-D-13-00650.1

Broecker, W. S. (1987, July). *Unpleasant surprises in the greenhouse?* http://dx.doi.org/10.1038/328123a0. (Accessed: 2023-7-27) doi: 10.1038/328123a0

Brovkin, V., Brook, E., Williams, J. W., Bathiany, S., Lenton, T. M., Barton, M., ... Yu, Z. (2021, July). Past abrupt changes, tipping points and cascading impacts in the earth system. *Nat. Geosci.*, *14*(8), 550-558. doi: 10.1038/s41561-021-00790-5

Caesar, L., McCarthy, G. D., Thornalley, D. J. R., Cahill, N., & Rahmstorf, S. (2021, March). Current atlantic meridional overturning circulation weakest in last millennium. *Nat. Geosci.*, *14*(3), 118-120. doi: 10.1038/s41561-021-00699-z

Caesar, L., Rahmstorf, S., Robinson, A., Feulner, G., & Saba, V. (2018, April). Observed fingerprint of a weakening atlantic ocean overturning circulation. *Nature*, *556*(7700), 191-196. doi: 10.1038/s41586-018-0006-5

Cheng, W., Chiang, J. C. H., & Zhang, D. (2013, September). Atlantic meridional overturning circulation (AMOC) in CMIP5 models: RCP and historical simulations. *J. Clim.*, *26*(18), 7187-7197. doi: 10.1175/JCLI-D-12-00496.1

Chiang, J. C. H., & Bitz, C. M. (2005, October). Influence of high latitude ice cover on the marine intertropical convergence zone. *Clim. Dyn.*, *25*(5), 477-496. doi: 10.1007/s00382-005-0040-5

Chiang, J. C. H., Cheng, W., & Bitz, C. M. (2008, April). Fast teleconnections to the tropical atlantic sector from atlantic thermohaline adjustment. *Geophys. Res. Lett.*, *35*(7). doi: 10.1029/2008gl033292

Danabasoglu, G., Lamarque, J.-F., Bacmeister, J., Bailey, D. A., DuVivier, A. K., Edwards, J., ... Strand, W. G. (2020, February). The community earth system model version 2 (CESM2). *J. Adv. Model. Earth Syst.*, *12*(2). doi: 10.1029/2019ms001916

Ditlevsen, P., & Ditlevsen, S. (2023, July). Warning of a forthcoming collapse of the atlantic meridional overturning circulation. *Nat. Commun.*, *14*(1), 4254. doi: 10.1038/s41467-023-39810-w

Donohoe, A., Marshall, J., Ferreira, D., & Mcgee, D. (2013, June). The relationship between ITCZ location and Cross-Equatorial atmospheric heat transport: From the seasonal cycle to the last glacial maximum. *J. Clim.*, *26*(11), 3597-3618. doi: 10.1175/JCLI-D-12-00467.1

Eyring, V., Bony, S., Meehl, G. A., Senior, C. A., Stevens, B., Stouffer, R. J., & Taylor, K. E. (2016, May). Overview of the coupled model intercomparison project phase 6 (CMIP6) experimental design and organization. *Geosci. Model Dev.*, *9*(5), 1937-1958. doi: 10.5194/gmd-9-1937-2016

Fasullo, J. T., Lamarque, J.-F., Hannay, C., Rosenbloom, N., Tilmes, S., DeRepentigny, P., ... Deser, C. (2022, January). Spurious late historical-era warming in CESM2 driven by prescribed biomass burning emissions. *Geophys. Res. Lett.*, *49*(2). doi: 10.1029/2021gl097420

Frierson, D. M. W., Hwang, Y.-T., Fučkar, N. S., Seager, R., Kang, S. M., Donohoe, A., ... Battisti, D. S. (2013, October). Contribution of ocean overturning circulation to tropical rainfall peak in the northern hemisphere. *Nat. Geosci.*, *6*(11), 940-944. doi: 10.1038/ngeo1987

Gettelman, A., & Morrison, H. (2015, February). Advanced Two-Moment bulk microphysics for global models. part i: Off-Line tests and comparison with other schemes. *J. Clim.*, *28*(3), 1268-1287. doi: 10.1175/JCLI-D-14-00102.1

Hassan, T., Allen, R. J., Liu, W., & Randles, C. A. (2021, April). Anthropogenic aerosol forcing of the atlantic meridional overturning circulation and the associated mechanisms in CMIP6 models. *Atmos. Chem. Phys.*, *21*(8), 5821-5846. doi: 10.5194/acp-21-5821-2021

Hoesly, R. M., Smith, S. J., Feng, L., Klimont, Z., Janssens-Maenhout, G., Pitkanen, T., ... Zhang, Q. (2018, January). Historical (1750–2014) anthropogenic emissions of reactive gases and aerosols from the community emissions data system (CEDS).

Geosci. Model Dev., *11*(1), 369-408. doi: 10.5194/gmd-11-369-2018

Holland, M. M., Hannay, C., Fasullo, J., Jahn, A., Kay, J. E., Mills, M., ... Bailey, D. (2023, August). *New model ensemble reveals how forcing uncertainty and model structure alter climate simulated across CMIP generations of the community earth system model.* doi: 10.5194/gmd-2023-125

Hurrell, J. W., Holland, M. M., Gent, P. R., Ghan, S., Kay, J. E., Kushner, P. J., ... Marshall, S. (2013, September). The community earth system model: A framework for collaborative research. *Bull. Am. Meteorol. Soc.*, *94*(9), 1339-1360. doi: 10.1175/BAMS-D-12-00121.1

Irving, D. B., Wijffels, S., & Church, J. A. (2019, May). Anthropogenic aerosols, greenhouse gases, and the uptake, transport, and storage of excess heat in the climate system. *Geophys. Res. Lett.*, *46*(9), 4894-4903. doi: 10.1029/2019gl082015

Kay, J. E., Deser, C., Phillips, A., Mai, A., Hannay, C., Strand, G., ... Vertenstein, M. (2015, August). The community earth system model (CESM) large ensemble project: A community resource for studying climate change in the presence of internal climate variability. *Bull. Am. Meteorol. Soc.*, *96*(8), 1333-1349. doi: 10.1175/BAMS-D-13-00255.1

Lamarque, J.-F., Bond, T. C., Eyring, V., Granier, C., Heil, A., Klimont, Z., ... van Vuuren, D. P. (2010, August). Historical (1850–2000) gridded anthropogenic and biomass burning emissions of reactive gases and aerosols: methodology and application. *Atmos. Chem. Phys.*, *10*(15), 7017-7039. doi: 10.5194/acp-10-7017-2010

Lembo, V., Folini, D., Wild, M., & Lionello, P. (2019, July). Inter-hemispheric differences in energy budgets and cross-equatorial transport anomalies during the 20th century. *Clim. Dyn.*, *53*(1), 115-135. doi: 10.1007/s00382-018-4572-x

Lenton, T. M., Rockström, J., Gaffney, O., Rahmstorf, S., Richardson, K., Steffen, W., & Schellnhuber, H. J. (2019, November). Climate tipping points - too risky to bet against. *Nature*, *575*(7784), 592-595. doi: 10.1038/d41586-019-03595-0

Liu, X., Ma, P.-L., Wang, H., Tilmes, S., Singh, B., Easter, R. C., ... Rasch, P. J. (2016, February). Description and evaluation of a new four-mode version of the modal aerosol module (MAM4) within version 5.3 of the community atmosphere model. *Geosci. Model Dev.*, *9*(2), 505-522. doi: 10.5194/gmd-9-505-2016

Marshall, J., Donohoe, A., Ferreira, D., & McGee, D. (2013). The ocean's role in setting the mean position of the Inter-Tropical convergence zone. *Clim. Dyn.*, *42*(7), 1967-1979. doi: 10.1007/s00382-013-1767-z

Menary, M. B., Robson, J., Allan, R. P., Booth, B. B. B., Cassou, C., Gastineau, G., ... Zhang, R. (2020, July). Aerosol-forced AMOC changes in CMIP6 historical simulations. *Geophys. Res. Lett.*, *47*(14). doi: 10.1029/2020gl088166

Needham, M. R., & Randall, D. A. (2023, June). Anomalous northward energy transport due to anthropogenic aerosols during the 20th century. *J. Clim.*, *-1*(aop), 1-37. doi: 10.1175/JCLI-D-22-0798.1

Pearce, F. A., & Bodas-Salcedo, A. (2023, May). Implied heat transport from CERES data: Direct radiative effect of clouds on regional patterns and hemispheric symmetry. *J. Clim.*, *36*(12), 4019-4030. doi: 10.1175/JCLI-D-22-0149.1

Rahmstorf, S. (2002, September). Ocean circulation and climate during the past 120,000 years. *Nature*, *419*(6903), 207-214. doi: 10.1038/nature01090

Rahmstorf, S., Box, J. E., Feulner, G., Mann, M. E., Robinson, A., Rutherford, S., & Schaffernicht, E. J. (2015, March). Exceptional twentieth-century slowdown in atlantic ocean overturning circulation. *Nat. Clim. Chang.*, *5*(5), 475-480. doi: 10.1038/nclimate2554

Robson, J., Menary, M. B., Sutton, R. T., Mecking, J., Gregory, J. M., Jones, C., ... Wilcox, L. J. (2022, October). The role of anthropogenic aerosol forcing in the 1850–1985 strengthening of the AMOC in CMIP6 historical simulations. *J. Clim.*, *35*(20), 3243-3263. doi: 10.1175/JCLI-D-22-0124.1

Rodgers, K. B., Lee, S.-S., Rosenbloom, N., Timmermann, A., Danabasoglu, G., Deser, C., . . . Yeager, S. G. (2021, December). Ubiquity of human-induced changes in climate variability. *Earth Syst. Dyn.*, *12*(4), 1393-1411. doi: 10.5194/esd-12-1393-2021

Speer, K., & Tziperman, E. (1992, January). Rates of water mass formation in the north atlantic ocean. *J. Phys. Oceanogr.*, *22*(1), 93-104. doi: 10.1175/1520-0485(1992)022⟨0093:ROWMFI⟩2.0.CO;2

Thornalley, D. J. R., Oppo, D. W., Ortega, P., Robson, J. I., Brierley, C. M., Davis, R., . . . Keigwin, L. D. (2018, April). Anomalously weak labrador sea convection and atlantic overturning during the past 150 years. *Nature*, *556*(7700), 227-230. doi: 10.1038/s41586-018-0007-4

Trenberth, K. E., & Caron, J. M. (2001, August). Estimates of meridional atmosphere and ocean heat transports. *J. Clim.*, *14*(16), 3433-3443. doi: 10.1175/1520-0442(2001)014⟨3433:EOMAAO⟩2.0.CO;2

Trenberth, K. E., & Fasullo, J. T. (2017, February). Atlantc meridional heat transports computed from balancing earth's energy locally. *Geophys. Res. Lett.*, *44*(4), 1919-1927. doi: 10.1002/2016GL072475

Wang, C., Soden, B. J., Yang, W., & Vecchi, G. A. (2021, February). Compensation between cloud feedback and aerosol-cloud interaction in CMIP6 models. *Geophys. Res. Lett.*, *48*(4). doi: 10.1029/2020gl091024

Yukimoto, S., Oshima, N., Kawai, H., Deushi, M., & Aizawa, T. (2022, September). Role of interhemispheric heat transport and global atmospheric cooling in multidecadal trends of northern hemisphere precipitation. *Geophys. Res. Lett.*, *49*(18). doi: 10.1029/2022gl100335

Figure 1.

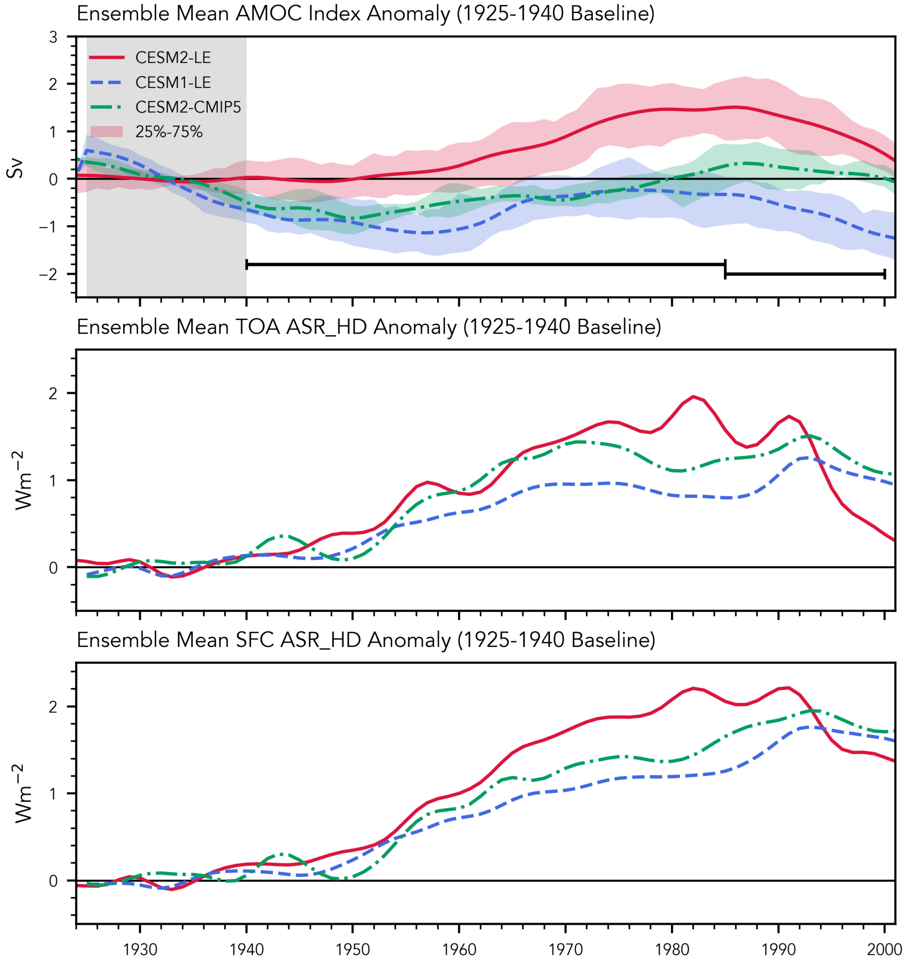
Ensemble Mean AMOC Index Anomaly (1925-1940 Baseline)
CESM2-LE
CESM1-LE
CESM2-CMIP5
25%-75%
Sv
3
2
1
0
−1
−2
Ensemble Mean TOA ASR_HD Anomaly (1925-1940 Baseline)
Wm^{-2}
2
1
0
Ensemble Mean SFC ASR_HD Anomaly (1925-1940 Baseline)
Wm^{-2}
2
1
0
1930
1940
1950
1960
1970
1980
1990
2000

Figure 2.

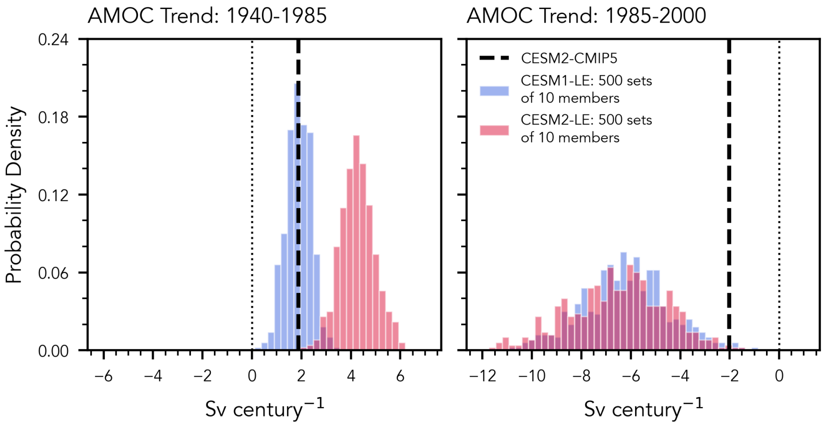

AMOC Trend: 1940-1985
AMOC Trend: 1985-2000
Probability Density
0.24
0.18
0.12
0.06
0.00
−6
−4
−2
0
2
4
6
Sv century^{-1}
CESM2-CMIP5
CESM1-LE: 500 sets of 10 members
CESM2-LE: 500 sets of 10 members
−12
−10
−8
−6
−4
−2
0
Sv century^{-1}

Figure 3.

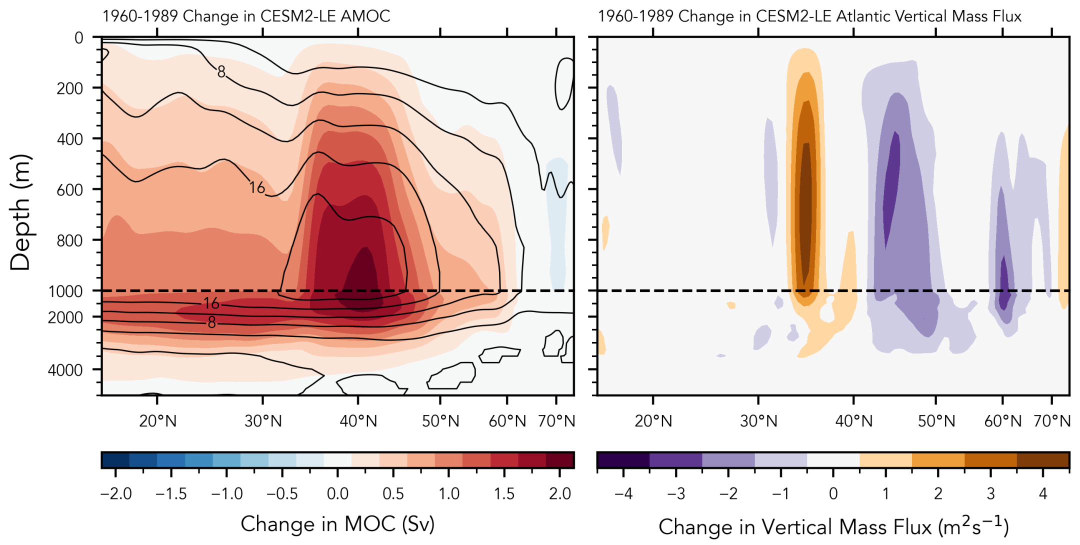

1960-1989 Change in CESM2-LE AMOC
1960-1989 Change in CESM2-LE Atlantic Vertical Mass Flux
Depth (m)
0
200
400
600
800
1000
2000
4000
8
16
16
8
20°N
30°N
40°N
50°N
60°N
70°N
−2.0
−1.5
−1.0
−0.5
0.0
0.5
1.0
1.5
2.0
Change in MOC (Sv)
−4
−3
−2
−1
0
1
2
3
4
Change in Vertical Mass Flux (m^2s^{-1})

Figure 4.

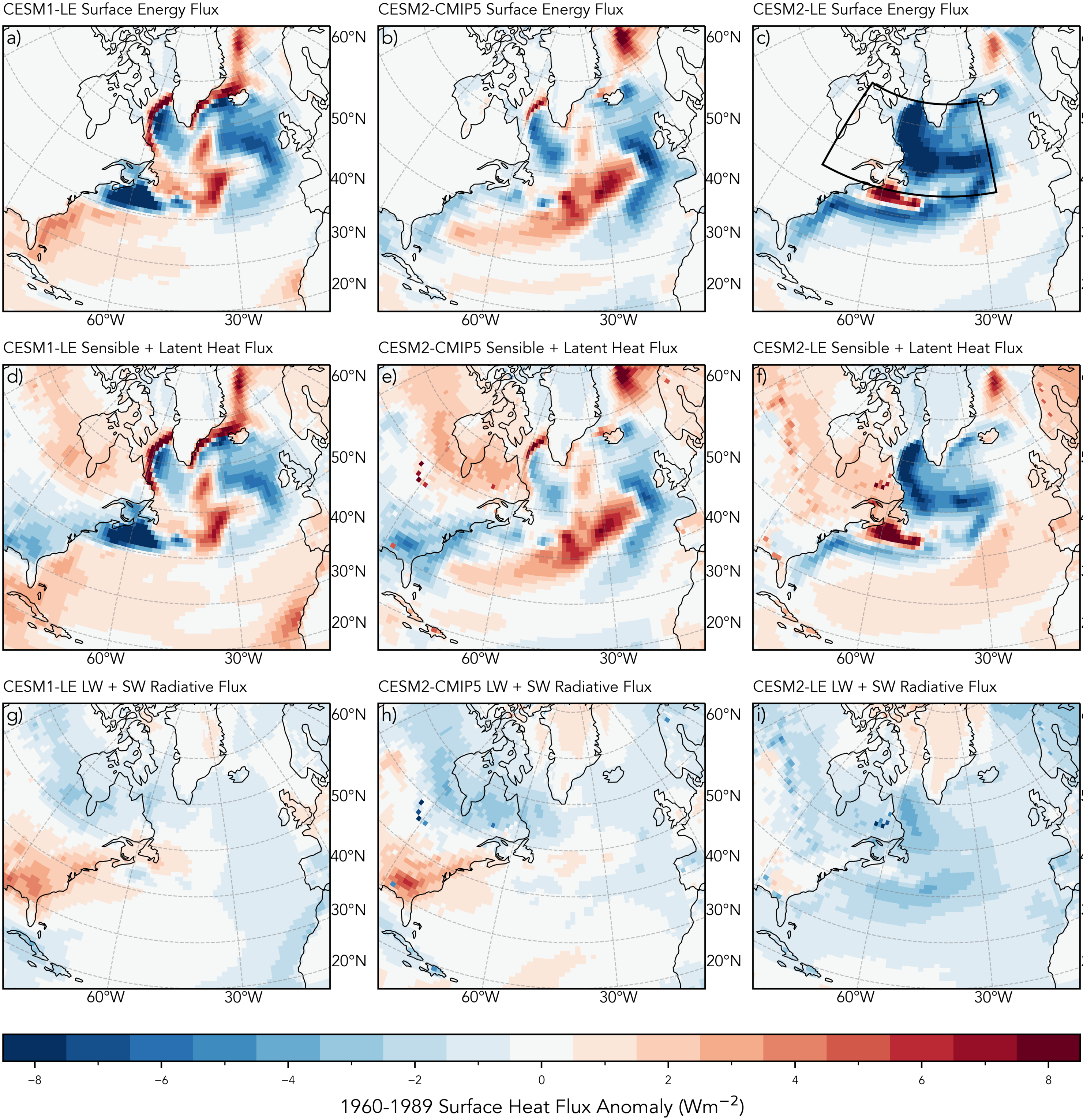

CESM1-LE Surface Energy Flux
CESM2-CMIP5 Surface Energy Flux
CESM2-LE Surface Energy Flux
a)
b)
c)
CESM1-LE Sensible + Latent Heat Flux
CESM2-CMIP5 Sensible + Latent Heat Flux
CESM2-LE Sensible + Latent Heat Flux
d)
e)
f)
CESM1-LE LW + SW Radiative Flux
CESM2-CMIP5 LW + SW Radiative Flux
CESM2-LE LW + SW Radiative Flux
g)
h)
i)
60°N
50°N
40°N
30°N
20°N
60°W
30°W
−8
−6
−4
−2
0
2
4
6
8
1960-1989 Surface Heat Flux Anomaly (Wm^{-2})

Figure 5.

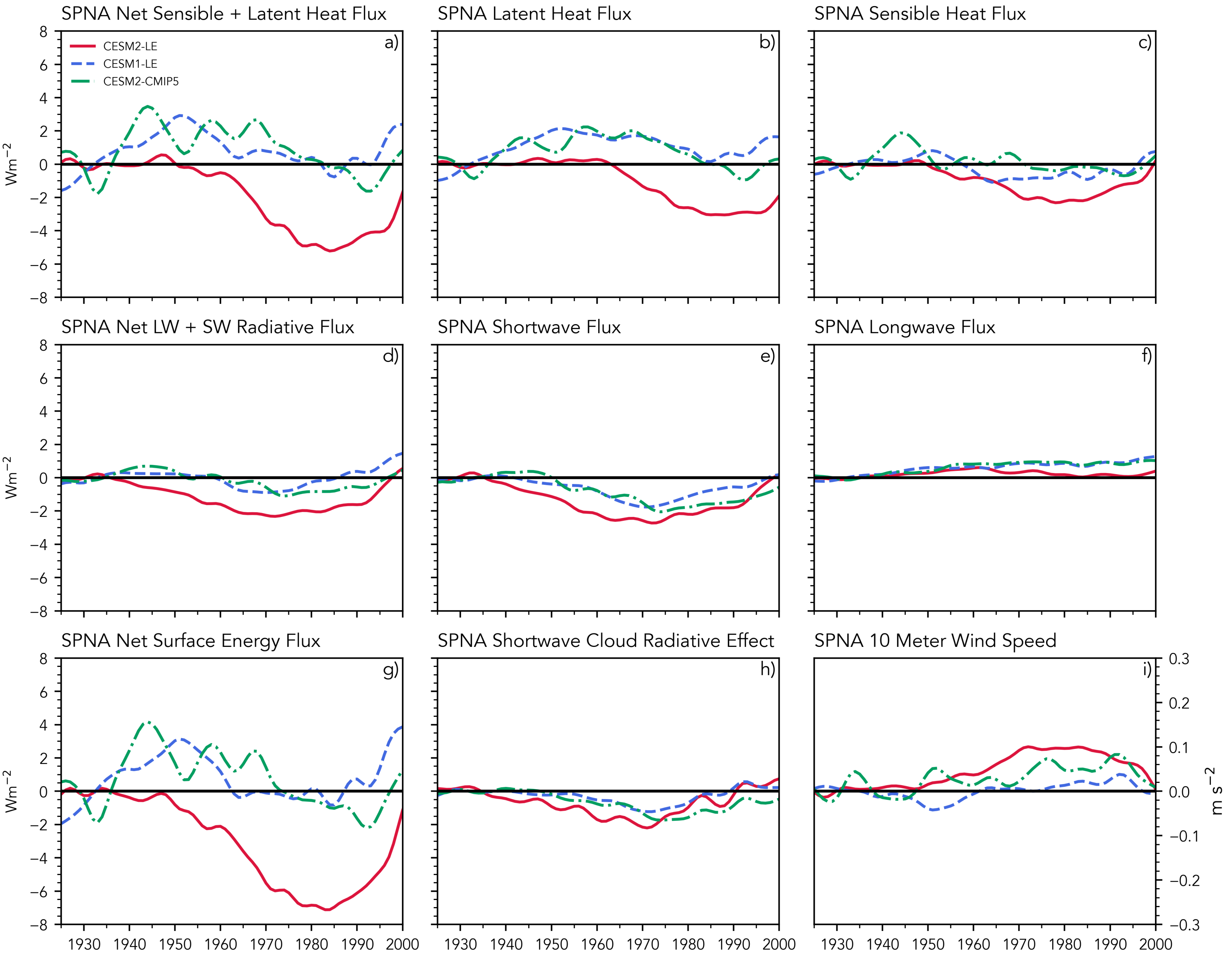

SPNA Net Sensible + Latent Heat Flux
SPNA Latent Heat Flux
SPNA Sensible Heat Flux
SPNA Net LW + SW Radiative Flux
SPNA Shortwave Flux
SPNA Longwave Flux
SPNA Net Surface Energy Flux
SPNA Shortwave Cloud Radiative Effect
SPNA 10 Meter Wind Speed
CESM2-LE
CESM1-LE
CESM2-CMIP5
a)
b)
c)
d)
e)
f)
g)
h)
i)
Wm⁻²
m s⁻²